6482 *Biochemistry* **2009,** *48,* 6482–6494
DOI: 10.1021/bi900526z

BIOCHEMISTRY
including biophysical chemistry & molecular biology
Article

Polarization and Polarizability Assessed by Protein Amide Acidity

Griselda Hernández,[‡] Janet S. Anderson,[§] and David M. LeMaster*[,‡]

[‡]*Wadsworth Center, New York State Department of Health, and Department of Biomedical Sciences, School of Public Health, University at Albany—SUNY, Empire State Plaza, Albany, New York 12201, and* [§]*Department of Chemistry, Union College, Schenectady, New York 12308*

Received March 27, 2009; Revised Manuscript Received June 7, 2009

ABSTRACT: Hydroxide-catalyzed exchange rate constants were determined for those amides of FK506-binding protein (FKBP12), ubiquitin, and chymotrypsin inhibitor 2 (CI2) that are solvent-accessible in the high-resolution X-ray structures. When combined with previous hydrogen exchange results for the rubredoxin from *Pyrococcus furiosus*, the acidity of these amides was calculated by continuum dielectric methods as a function of the nonpolarizable electrostatic parameter set, internal dielectric, and the charge distribution of the peptide anion. The CHARMM22 parameter set with an internal dielectric value of 3 and an ab initio-derived anion charge distribution yielded an rmsd value of 7 for the 56 amide exchange rate constants ranging from $10^{0.67}$ to $10^{9.0}$ M^{-1} s^{-1}. The OPLS-AA parameter set yielded comparably robust predictions, while that of PARSE, AMBER parm99, and AMBER ff03 performed more poorly. The small value for the optimal internal dielectric, combined with the brief lifetime of the peptide anion intermediate and the uniformity of the correlation between predicted and observed amide acidities, is consistent with electronic polarizability providing the dominant contribution to dielectric shielding. By construction, nonpolarizable force fields do not model electric field attenuation by electronic polarizability. Accurate prediction of the total electrostatic energy by such force fields necessitates the hyperpolarization of the atomic charge values in order to match the average electric field energy density $(1/2)\varepsilon(\tau)E^2(\tau)$ when $\varepsilon(\tau)$ is set to the in vacuo dielectric value of 1. The resulting predictions of the experimental hydrogen exchange data demonstrate the substantial systematic errors in the predicted electrostatic potential that can arise when dielectric shielding due to electronic polarizability is neglected.

Protein amide hydrogen exchange rates are commonly used to estimate the free energy of the conformational transitions that generate solvent exposure for structurally buried amides. Central in the standard analysis (*1*) is the assumption that exposure to solvent results in amide exchange rates that are equal to those for simple model peptides. Yet, amide hydrogens that are exposed to solvent in high-resolution protein X-ray structures exhibit at least a 3×10^9-fold range in exchange rates, relative to the model peptide values (*2*, *3*). Such a 3 billion-fold variation corresponds to a 13 kcal/mol difference in apparent conformational stability. This range in free energy is as large as the maximal global stability of any protein predicted from hydrogen exchange measurements that has been independently verified by either calorimetric or spectroscopic methods (*4*, *5*).

The exchange rates for the static solvent-exposed amides of *Pyrococcus furiosus* (*Pf*)[1] rubredoxin span a billion-fold range (*2*). Drawing on earlier observations that electrostatic solvation free energy calculations can serve to predict the kinetics of hydrogen exchange in model peptides (*6*, *7*), with one exception, we (*2*) found that Poisson−Boltzmann predictions of acidities for the solvent-exposed amides of *Pf* rubredoxin agree with the observed hydrogen exchange rate constants to within an rmsd of 6 using the nonpolarizable CHARMM22 (*8*) electrostatic parameters. Interestingly, the optimal value for the effective internal dielectric was found to be 3, far below the dielectric shielding values that have been obtained in analogous predictions of protein side chain titrations. Optimal internal dielectric values near 20 have commonly been obtained when Poisson−Boltzmann analysis is applied to the full set of experimentally determined side chain titrations (*9*, *10*). Similar results have been obtained for the subset of strongly shifted side chain titrations. Identical electrostatic analyses of seven different proteins for side chains having p*K* values shifted by at least 2 units yielded internal dielectric values ranging from 10 to 23 (*11*).

Protein conformational reorganization through reorientation of mobile charged side chains provides the primary contribution to the comparatively high dielectric shielding observed for the ionizable side chains (*12*), although larger scale structural motion can play a critical role, particularly for buried side chains (*13*). The efficient dielectric shielding provided by conformational reorganization is dependent upon the long lifetime of the ionized

*To whom correspondence should be addressed. E-mail: lemaster@wadsworth.org. Tel: 518-474-6396. Fax: 518-473-2900.

[1]Abbreviations: FKBP12, human FK506-binding protein; CI2, barley chymotrypsin inhibitor 2; *Pf*, *Pyrococcus furiosus*; IPTG, isopropyl thiogalactoside; EDTA, ethylenediaminetetraacetate; CLEANEX-PM, clean chemical exchange-phase modulated; DFT, density functional theory; PCM, polarizable continuum model.

 Published on Web 06/09/2009

side chain state. Neutral carboxyl, amine, and imidazole side chains react with hydroxide and hydronium ion at diffusion-limited rates ($\sim 10^{10}\ M^{-1}\ s^{-1}$), while the reverse process of proton donation to, or removal from, a neutral water molecule occurs at a rate determined by the side chain pK value. As a result, these ionized side chains have lifetimes in the range of microseconds to milliseconds near neutral pH, and all of the conformational dynamics that occur within this time frame can potentially contribute to the dielectric shielding of the charged state. It may be noted that electric field fluctuations in the millisecond time frame have been proposed to contribute to the similar temporal distribution of enzyme catalysis rates determined from single molecule measurements (*14*).

The kinetic dependence of the hydroxide-catalyzed amide hydrogen exchange reaction is the reverse of what is observed for the ionizable side chains. Since, in nearly all cases, the acidity of the protein peptide backbone is less than the acidity of the neutral water molecule, the reaction rate of an amide with hydroxide ion is attenuated from the diffusion limit ($2 \times 10^{10}\ M^{-1}\ s^{-1}$ at 25 °C (*15*, *16*) by the fraction of forward-reacting encounters $K_i/(K_i + 1)$, where K_i is the equilibrium constant for the transfer of a proton from the amide to an hydroxide ion. Conversely, since amides react as normal Eigen acids (*17*), essentially every encounter between the amide anion and a neutral water molecule is expected to give rise to a proton transfer, resulting in a very short lifetime for the amide anion state. In analogy to the proton transfer rates that have been measured for photoactivated strong acids (*18*, *19*) and bases (*20*), as well as for the hydronium ion (*21*), a solvent-exposed peptide anion intermediate is expected to be quenched by a neutral water molecule in ~10 ps (*22*). The lifetimes for these proton transfers correspond closely with the $(8\ ps)^{-1}$ rate for the dominant Debye dielectric relaxation mode in bulk phase water (*23*), and this solvent reorganization has been proposed to be rate-limiting for such proton transfer reactions (*18*).

Analogous to the transient charge states that can occur in electron transfer reactions (*24*), the brief lifetime of the peptide anion strongly limits the magnitude of protein conformational reorganization that can significantly contribute to the dielectric shielding of that anion. Even unhindered side chain rotamer transitions generally occur at rates that are 10−100-fold slower than the rate of peptide anion quenching by neutral water. This brief time window for dielectric response to the ionization of the peptide implies that in most cases the structure surrounding the peptide anion will be well represented by that of the un-ionized state.

The effective internal dielectric value of 3 observed for the static solvent-accessible amides of *Pf* rubredoxin is consistent with electronic polarizability providing the dominant contribution to dielectric shielding of the peptide anion. If this correlation were to be established more generally with a larger set of proteins, these experimental hydrogen exchange data will provide a valuable basis on which to assess reliability among the commonly used nonpolarizable force field parameter sets and a practical testbed for evaluating the ongoing development of polarizable force fields.

More fundamentally, if conformational reorganization does not contribute significantly to the dielectric shielding of protein peptide anion, then why does the optimal dielectric shielding in these continuum dielectric calculations occur at a value of $\varepsilon_{int} = 3$? For the widely used nonpolarizable force fields, the electrostatic parameters are optimized to calculate total energy under the assumption of no background dielectric (i.e., $\varepsilon_{int} = 1$). In such calculations, dielectric shielding can only be modeled by the rotational and translational motions of conformational reorganization. In reality, dielectric shielding in proteins also arises from the rapid redistribution of electron density in response to a change in the electric field. The atomic charge values used in the nonpolarizable force fields are hyperpolarized with respect to gas phase calculations, so as to mimic the average degree of polarization that occurs in the condensed phase. However, the electric field attenuation that results from electronic polarizability is ignored in such calculations.

Refractive index measurements yield optical dielectric values near 2.0 for typical organic liquids. Drawing upon these results, the contribution to protein dielectric shielding arising from electronic polarizability has commonly been set to this value in electrostatic calculations. However, the density within a protein is 30−40% higher than that of analogous small molecule organic liquids (*25*, *26*). As a result, the average optical dielectric value for protein molecules is at least 2.5 (*27*). On the slower time scale of $\sim 10^{-13}$ s, the nuclei respond to the altered electron density distribution and electric field by adjusting bond lengths and vibrational frequencies. Although estimates vary, the nuclear relaxation response may account for as little as 5% of the total polarizability (*28*).

The dielectric shielding effect of nuclear relaxation is also largely unaccounted for in the standard nonpolarizable force field calculations. Fixed bond lengths are typically used in such simulations. Furthermore, the electrostatic interactions between geminal atoms that would modulate bond angle fluctuations are set to zero, and those between 1 and 4 linked atom pairs are typically scaled down so that electric field effects on torsional angle fluctuations are attenuated.

We report hydrogen exchange measurements on human FK506-binding protein (FKBP12), human ubiquitin, and chymotrypsin inhibitor 2 from barley (CI2). This expanded set of experimental data provides a more definitive basis for assessment of (i) the contribution of electronic polarizability to dielectric shielding of protein peptide anions, (ii) the robustness of various nonpolarizable force field parametrizations, and (iii) the distribution of the excess negative charge of the amide anion among the atoms of the peptide unit. Analysis of the dependence of these peptide acidity predictions upon the value of the effective internal dielectric provides a means to assess the roles of polarization and polarizability in the prediction of protein electrostatic interactions.

EXPERIMENTAL PROCEDURES

Gene Expression Design. Genes for the human FK506-binding protein, human ubiquitin, and barley chymotrypsin inhibitor 2 gene were chemically synthesized (Genscript) from the wild-type gene sequence, with codon optimization for expression in *Escherichia coli*. The genes were cloned into the expression vector pET11a and then transformed into the BL21-(DE3) strain (Novagen) for expression. The FKBP12 gene was substituted with the C22V mutation for enhanced chemical stability of the protein. Valine is by far the most common substitution for this position among the closest evolutionary relatives of humans, with 27 of the top 100 protein−protein alignments in a nonredundant BLASTP (*29*) search of the NCBI database containing a valine substitution (all above 70% total sequence identity). The four alanine replacements were the only

other residue substitutions observed within the top 100 alignments. When the valine side chain was modeled in the 0.92 Å resolution X-ray structure of FKBP12 (PDB code 2PPN (*30*)) with a χ_1 torsion angle of 168°, the closest van der Waals contacts of the valine methyl groups were 3.1 Å to both Val 24 $C^{\gamma 1}$ and Leu 103 $C^{\delta 1}$. Given that the first 19 residues of the CI2 protein are disordered in the X-ray structure of the full-length inhibitor (*31*), Leu 20 was mutated to Met for translational initiation at that site so as to produce a truncated 62 residue form that is known to retain structure and inhibitory function (*32*).

Protein Purification. Protein expression and the initial stages of purification were handled similarly for FKBP12, ubiquitin, and CI2. BL21(DE3) cells containing the expression gene in pET11a were grown in minimal ^2H_2O medium containing 0.2% [U-^{2}H]glycerol as carbon source and 0.1% $^{15}NH_4Cl$ as nitrogen source, as previously described (*33*). For ubiquitin and CI2 the cells were grown at 37 °C to an OD_{600} of 0.7, at which point 0.5 mM IPTG was added. Following agitation overnight at 37 °C, the cells were concentrated by centrifugation and frozen at −80 °C. In the FKBP12 expression, the growth flasks were chilled to 25 °C before IPTG induction, and expression was continued overnight at 25 °C before centrifugation and freezing of the cells. For each protein, the frozen cells were thawed and resuspended in a buffer containing 50 mM Tris base, 30 mM acetic acid, and 1 mM EDTA. After treatment with hen lysozyme for 20 min on ice, $MgCl_2$ and $CaCl_2$ were added to a final concentration of 10 and 5 mM, respectively, and solid DNase I was added. After DNA digestion for 15 min, the cell suspensions were sonicated and the samples centrifuged at 35000*g* for 20 min. Following a 40% ammonium sulfate fractionation, the crude protein was recovered in a 90% ammonium sulfate fractionation and then redissolved and loaded onto a Sephadex G-50 gel filtration column equilibrated in the 50 mM Tris base and 30 mM acetic acid buffer.

The gel filtration fractions for the FKBP12 purification were diluted 2-fold and adjusted to pH 5.5 with acetic acid. Following loading onto a SP-Sepharose FF ion-exchange column equilibrated in 20 mM Tris−acetate, pH 5.5, the FKBP12 sample was eluted in a 0−600 mM NaCl gradient (*34*). The gel filtration fractions for the ubiquitin purification were adjusted to pH 5.0 with acetic acid. Following loading onto a SP-Sepharose FF ion-exchange column equilibrated in 30 mM Tris−acetate, pH 5.0, the ubiquitin sample was eluted in a 0−400 mM NaCl gradient (*35*). The gel filtration fractions for the CI2 purification were consecutively passed through a Sephadex QAE-A25 ion-exchange column and a SP-Sepharose FF ion-exchange column, both of which were equilibrated in the initial buffer containing 50 mM Tris base and 30 mM acetic acid.

NMR Sample Preparation and Data Collection. For each protein, aliquots of a U-^{2}H,^{15}N-enriched sample were concentrated and then exchanged into a series of buffers, via centrifugal ultrafiltration, to a final protein concentration of ∼2 mM. Acetate (for pH values below 6), phosphate (for pH values between 6 and 8), borate (for pH values up to 10), and carbonate (pH values above 10) buffers at 20 mM concentration in 6% ^2H_2O were adjusted to a total ionic strength of 150 mM with sodium chloride. Clean chemical exchange-phase modulated (CLEANEX-PM) (*36*) spectra with relaxation compensation (*37*) were collected on a Bruker Avance DRX 500 MHz spectrometer at 25 °C with mix times of 6.49, 12.98, 21.41, 32.44, and 51.90 ms as previously described (*38*). The intensity of each fully relaxed spectrum was estimated by exponential extrapolation of the intensities from the hard pulse reference experiment using relaxation delays of 2.0, 4.0, and 8.0 s.

Continuum Dielectric Calculations. Hydrogen atoms were added to the X-ray coordinate sets with the program Reduce (*39*). Hydroxyl hydrogens for which no specific hydrogen bond acceptor is apparent were directed toward the solvent phase with a trans orientation of the terminal side chain torsion angle. The coordinate sets 1BQ8 (*40*), 2PPN (*30*), and 1LW6 (*41*) were used for the electrostatic calculations on *Pf* rubredoxin, FKBP12, and CI2, respectively. The C22V mutation was computationally introduced into the FKBP12 coordinate set as described above, and the internally coordinated water molecule Wat3 (*30*) was added and parametrized according to the TIP3P model (*42*). The unpublished coordinates for a 1.00 Å X-ray structure of a K29Q variant of ubiquitin were kindly provided by S. Ramaswamy (University of Iowa) and A. D. Robertson (Keystone Symposia). A citation of this structure has been previously published (*43*). Since the hydrogen bond between the Gln 29 side chain and the amide hydrogen of Glu 16 does not exist in the wild-type ubiquitin structure, the side chain of residue 29 was converted to an alanine in the peptide acidity calculation for Glu 16. Although identified as a wild-type sequence in the structural report (*41*), the CI2 protein sequence in the 1LW6 PDB file contains a E26A mutation, relative to the more widely studied form. Asp 45 is the only static solvent-exposed amide within 8 Å of the Glu 26 carboxylate in the lower resolution 2CI2 structure (*31*). Even discounting the Asp 45 amide, Poisson−Boltzmann calculations using the 2CI2 X-ray structure yield a poorer prediction of the experimental log k_{OH^-} values than that provided by the 1LW6 structure.

Nonlinear Poisson−Boltzmann calculations were carried out using the DelPhi algorithm (*44*) with CHARMM22 (*8*), OPLS-AA (*45*), PARSE (*46*), AMBER parm99 (*47*), and AMBER ff03 (*48*) atomic charge and atomic radius parameter sets. For the OPLS-AA calculations the atomic radii were scaled to the Lennard-Jones parameter according to $\sigma_{ii} = 2^{-1/6}R$, with the exception of the polar hydrogen radii which were set to 0.05 Å. Atomic charges for the rubredoxin metal (Zn(II)) site were assigned as previously described (*2*). The protein termini and the lysine, arginine, aspartate, and glutamate residues were set to the charged state. Except where noted otherwise, the solvent dielectric value was set to 78.5 with the ionic strength set to the experimental value of 0.15 M. All DelPhi parameters, including the grid spacing of 0.25 Å, were applied as previously described (*2*), except that a 50% fill value was used. To facilitate comparisons between protein amide anions based on differing side chain conformations, in each calculation an *N*-methylacetamide (or *N*-methylacetamide anion) molecule was added to the continuum dielectric lattice volume such that the distance between the *N*-methylacetamide nitrogen and the nearest formal charge is at least 16 Å and no intermolecular atomic distance is less than 8 Å (*49*).

Poisson−Boltzmann calculations were carried out for those amide hydrogens that have static solvent accessibilities > 0.5 Å^2 using the default atomic radii of the ACCESS program (*50*). The X-ray structures used for the FKBP12 and ubiquitin calculations have a number of side chains with A and B conformers. Electrostatic calculations were carried out on each set, and for those amides that have static solvent accessibilities > 0.5 Å^2 in both conformer sets, the conformer that predicted the stronger peptide acidity was used in the subsequent analysis. The 1LW6 structure of CI2 is for a complex with subtilisin. Since the

NMR analysis was carried out on the free protein, only amide hydrogens having static solvent accessibilities >0.5 Å^2 in both the 1LW6 and lower resolution 2CI2 structures were analyzed.

Ab Initio Modeling of the N-Methylacetamide Anion Charge Distribution. Ab initio MP2 and B3LYP (*51*) density functional theory calculations using Gaussian03 (*52*) were initially carried out on *N*-methylacetamide and the *N*-methylacetamide anion at the aug-cc-pVDZ basis set level in vacuo and with PCM solvation at dielectric values of 3 and 78.39. Tight SCF convergence criteria were used for charge calculations. Starting from quantum mechanically refined coordinates (*53*), the structure was optimized at each level, and the Mulliken and ESP atomic charge distributions were calculated. B3LYP DFT calculations were subsequently carried out at the aug-cc-pVTZ basis set level, and these results were used to estimate the differential charge distribution of the anion.

RESULTS AND DISCUSSION

Amide Hydrogen Exchange at the Protein Surface. Rapid hydrogen exchange can be detected by NMR magnetization transfer techniques in which the water resonance is selectively excited, and the transfer of this magnetization to the amide resonances is then monitored. CLEANEX-PM is a particularly robust pulse sequence which efficiently suppresses NOE/ROE and TOCSY-derived contributions to the observed resonances (*36*), so as to yield signals that are solely derived from chemical exchange processes. We have introduced a modification to this experiment that compensates for the effects arising from transverse relaxation which, when uncorrected, limit the accuracy of the deduced exchange rates (*37*).

Relaxation-compensated CLEANEX-PM experiments were carried out on CI2, FKBP12, and ubiquitin at 25 °C in 0.15 M ionic strength buffers ranging from pH 5.5 to above pH 10. CI2 contains no histidines that otherwise might be expected to titrate within this pH range. The p*K* values of all side chain carboxyls in CI2 are below 5 (*54*). Consistent with an absence of side chain titration under neutral to moderately basic conditions, none of the static solvent-exposed amide hydrogens in CI2 exhibit deviations from a slope of 1.0 which is characteristic of a simple linear hydroxide-dependent exchange rate behavior over the range from pH 5.5 to pH 10 (Figure 1A). As a result, the kinetics for these amides over this pH range are completely characterized by the second-order rate constant for hydroxide-catalyzed exchange ($k_{OH^-} = k_{ex}/[OH^-]$). As noted in the earlier *Pf* rubredoxin study (*2*), a decreased slope in the $[OH^-]$ dependence near pH 11 is likely due primarily to the increasingly negative protein charge arising from the neutralization of lysine side chains.

The p*K* values of all side chain carboxyls in ubiquitin are below 4.5 (*55*). Although, as discussed below, both FKBP12 and ubiquitin contain histidine side chains, the large majority of the static surface-exposed amides in these two proteins exhibit a linear rate dependence of k_{ex} on hydroxide ion concentration over the range from pH 5.5 to pH 10. Due to the lack of a detailed structural model, residues of the dynamically disordered C-terminal tail of ubiquitin (*56*) were not included in this analysis. To enhance the chemical stability of FKBP12 at higher pH values, we introduced the evolutionarily conserved substitution of valine for Cys 22. The 23 solvent-exposed amides of FKBP12 and ubiquitin for which CLEANEX-PM measurements at two or more pH values demonstrated simple $[OH^-]$ rate dependencies are illustrated in panels B and C of Figure 1, respectively.

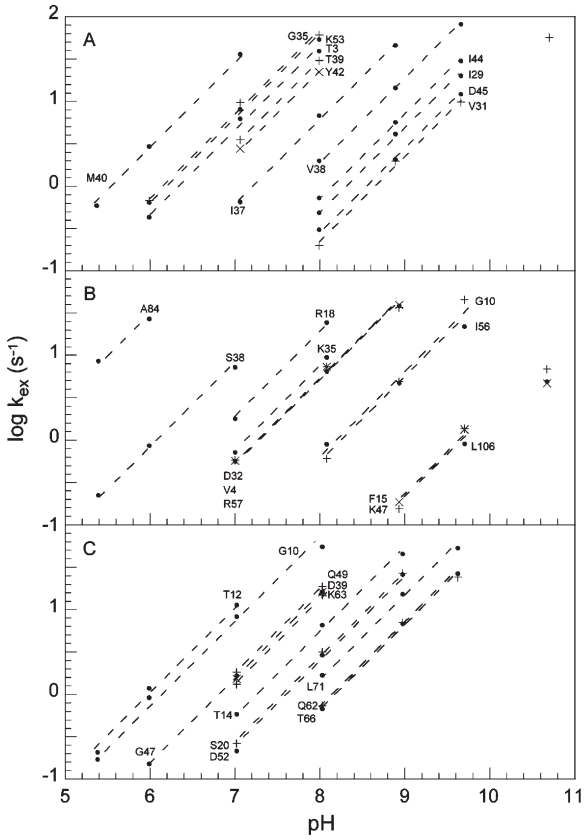

FIGURE 1: Magnetization transfer-based hydrogen exchange rate measurements on static solvent-exposed amides. CLEANEX-PM (*36*, *37*) measurements on CI2 (A), FKBP12 (B), and ubiquitin (C) were carried out at 25 °C. Data are plotted for static solvent-accessible amide hydrogens in which rate measurements were obtained at two or more pH values that conform to a simple hydroxide ion dependence for the exchange reaction. Not included are the residues adjacent to the N-terminus and the last four disordered residues of the ubiquitin sequence.

For all of these hydrogen exchange data, the rate determinations at each pH value are derived at five different CLEANEX-PM mix times, each of which provides an independent measurement of the exchange rate (*37*). Accurate exchange rates are obtained over a 500-fold range from 0.15 to 75 s^{-1}. When the present results are combined with the previously published data for *Pf* rubredoxin collected under analogous conditions (*2*), a total of 46 residues are found for which a linear hydroxide-dependent rate constant can be reliably fitted at two or more pH values with an overall uncertainty of 0.053 in the log k_{OH^-} rate constants. In the data analysis below, there are seven residues from the four proteins for which accurate exchange rates were obtained at only one pH value due to rate measurements at the pH extremes (Asp 14 and Val 38 of rubredoxin, Arg 62 of CI2, and Leu 106 of FKBP), resonance overlap (Val 60 of CI2 and Thr 6 of FKBP), or peak attenuation from conformational exchange broadening (Gly 53 of ubiquitin). The hydroxide-catalyzed second-order rate constants for the reported static solvent-accessible amides of FKBP, ubiquitin, and CI2 are available in Tables S1−S3 in the Supporting Information.

FKBP12 has three histidines, His 25, His 87, and His 94, with p*K* values of ≤ 3.6, 5.92, and 5.84, respectively (*57*). His 68 of ubiquitin has a p*K* value of 5.92 (*58*). Four solvent-exposed amides exhibit exchange behavior that is perturbed by ionization of these histidine side chains within the pH range of 5.5−10. The Henderson−Hasselbach dependence of the exchange rates for

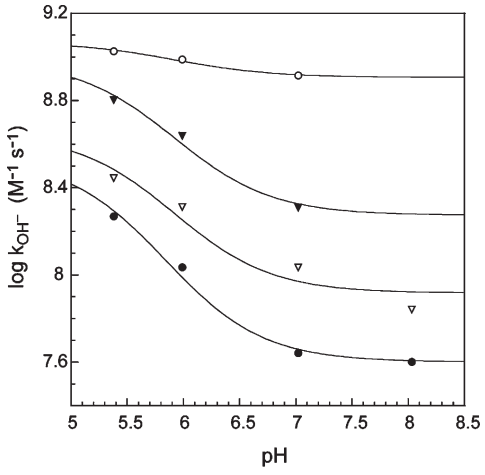

FIGURE 2: pH dependence of hydroxide-catalyzed amide exchange constants for residues perturbed by nearby histidine ionizations in FKBP12 and ubiquitin. A Henderson−Hasselbach dependence was fitted to the titration data of FKBP12 Thr 85 (●) and Gly 89 (○), given the pK values of 5.92 and 5.84 for His 87 and His 94, respectively (*57*), and to the titration data of ubiquitin Leu 8 (▽) and Ala 46 (▼), given the pK value of 5.92 for His 68 (*69*).

these four residues allows the log k_{OH^-} rate constants for the neutral imidazole charge state to be estimated (Figure 2). Similarly, the pH dependence of hydrogen exchange for Glu 16 of ubiquitin yields a log k_{OH^-} value of 6.3 for the charged N-terminal state of the protein in which the side chain carboxylate of Glu 16 forms a salt bridge with the N-terminal ammonium group in the X-ray structure.

The utility of determining the second-order rate constants of hydrogen exchange for the dominant charge configuration of a protein near physiological pH conditions is not limited to the present application. The vast majority of protein molecular dynamics simulations are run under the conditions of a fixed formal charge distribution. Although molecular dynamics protocols that model ionization transitions have been described, the long lifetime of the charge states for the ionizable side chains generally precludes adequate sampling of ionization events in an unconstrained simulation. Indeed, within the time frame of typical unconstrained molecular simulations, the various formal charge states of a protein generally represent distinct conformational dynamics manifolds. The gating of protein conformational transitions by side chain ionizations is widespread in biological systems. Much attention has focused upon the use of histidine ionization in the dynamical gating in phenomena such as electron transfer (*59*), enzymatic catalysis (*60*), and protein−protein signal transduction (*61*). However, other types of side chain ionization are likewise amenable to dynamical gating functions. Establishment of a set of protein systems in which the hydrogen exchange behavior of a specific formal charge configuration is characterized will facilitate the more complete interpretation of the structural and dynamical properties of such protein charge states.

Dominant Acidic Conformer Analysis in Hydrogen Exchange Prediction. Poisson−Boltzmann dielectric continuum predictions of peptide acidities were carried out for CI2, ubiquitin, and FKBP12 using the DelPhi program (*44*). The electrostatic solvation free energy was calculated for a series of protein structures that differ from each other only by which solvent-exposed amide has had its proton removed. If chemical induction effects do not differentially alter the intrinsic acidity of the protein amides, the difference in electrostatic solvation free energy for each such pair of amide anions will correspond to the free energy of transferring an amide hydrogen from one site to the other, which is proportional to the ΔpK for those two amide nitrogens (*2*). The free energy of this proton transfer is necessarily equivalent to the difference in free energy of protonating each amide anion site, since in both cases the identical neutral backbone protein structure is generated. As observed in the previous *Pf* rubredoxin study (*2*), the amide ΔpK values reflect both the intramolecular electrostatic interactions between the individual amide anions and the protein fixed atomic charges as well as the reaction field response of the low dielectric volume embedded in the high dielectric solvent phase. To deal with the situations discussed below in which individual protein side chains are altered, an *N*-methylacetamide molecule was introduced into the lattice volume of each continuum dielectric calculation to provide a common internal referencing of the electrostatic solvation free energy values (*49*).

Suitable continuum dielectric calculations depend upon the selection of an appropriate structural model. In this study, we have chosen the highest resolution X-ray structure available for each protein considered. In specific instances, the atomic coordinates of the X-ray structure yield electrostatic solvation free energy predictions that indicate a significantly slower hydrogen exchange rate than is experimentally observed. As described in the analysis of *Pf* rubredoxin hydrogen exchange (*2*), the χ_1 side chain torsion angles of Asp 21 and Asp 36 are oriented near −60° in the high-resolution X-ray structure (*40*). In both cases, the negatively charged carboxylate group is within 3 Å of the intraresidue amide hydrogen. Poisson−Boltzmann calculations on the resultant strong interaction with the peptide anion intermediate predict a far slower hydrogen exchange rate than is experimentally observed. Since the X-ray structure presents little hindrance to rotation of those side chains into the trans χ_1 rotamer, to predict the acidities of the Asp 21 and Asp 36 amides, we carried out electrostatic potential calculations in which only the intraresidue side chain is reoriented to a trans conformation. The trans rotamer caculations predicted hydrogen exchange rates that were 10^3- and 10^5-fold faster than for the gauche$^-$ χ_1 side chain conformers of Asp 21 and Asp 36, respectively, and the predicted rates for the trans rotamers closely agreed with the experimental exchange data (*2*).

The use of a single energetically accessible protein conformer with enhanced amide acidity as the model for electrostatic solvation free energy calculations raises several issues, in addition to the familiar question of how closely the crystal structure represents the dominant conformation in solution. Although population averaging of the conformer acidities ($\sum K_i$) is more formally correct (*62*), population averaging of the conformer pK_i values ($\sum pK_i$ or, equivalently, averaging of the conformer electrostatic potential values) has occasionally been used to estimate the effect of conformer sampling in the prediction of protein side chain ionization. In a detailed analysis of side chain ionizations in bovine pancreatic trypsin inhibitor and hen egg white lysozyme, Karplus and co-workers (*63*) concluded that, in assessment of the ionization midpoint for each titrating residue, averaging over the K_i values or averaging over the log K_i values usually has little effect on the predicted pK values.

The issue of K_i vs pK_i averaging is markedly different in the estimation of hydroxide-catalyzed hydrogen exchange rates near neutral pH where, in most cases, less than 1 out of every 10^{10} molecules will have a given amide in the ionized state. As a result,

whenever there is a substantial range in conformer acidities, the most acidic conformers can make the dominant contribution to the observed hydrogen exchange rate, even if they constitute only a modest fraction of the overall conformer population. We (*49*) recently analyzed the distribution of peptide acidities that are predicted for the set of Ala-Ala, Ala-Gly, Gly-Ala, and trans-Pro-Ala dipeptide conformations in the Protein Coil Library of Rose and colleagues (*64*) as a representation of the conformational distribution of simple peptides in solution. In each case, a million-fold range is predicted for the individual conformer acidities using an internal dielectric value of 3. Yet, the far smaller differences in experimental exchange rate among these model peptides are accurately predicted by averaging over the conformer acidities. The subset of acidic Ala-Ala conformers with an extended N-terminal residue and a C-terminal residue in an α conformation is predicted to account for over 60% of the total hydrogen exchange while constituting only 12% of the population. In contrast, over half of the Ala-Ala peptides in the coil library have either both residues in the extended conformation or both in the α conformation. However, when combined, these two sets of conformers are predicted to account for only 11% of the total hydrogen exchange reaction. When such an analysis is applied to the far more restricted backbone conformational dynamics of a native state protein, a single backbone conformer may often be expected to provide the dominant contribution to the observed exchange behavior.

In carrying out the Poisson−Boltzmann analysis of FKBP12, ubiquitin, and CI2, we noted a second type of systematic modulation in the peptide anion electrostatic solvation free energies as a function of the residue side chain conformation. When the χ_1 side chain torsion angle is near +60°, the γ atom is gauche to both the main chain nitrogen and carbonyl carbon. As a result of steric interactions with the main chain atoms, for most residue types this gauche$^+$ χ_1 rotamer is significantly disfavored, relative to the gauche$^-$ and trans states. In the gauche$^+$ rotamer with the main chain ϕ torsion angle near −90°, the $\beta-\gamma$ bond is approximately parallel to the N−H bond of the amide, thus placing the C$^\gamma$ close to the amide hydrogen (Figure 3). Given that the large majority of residues have ϕ angles in the range of −40° to −130°, a side chain with a χ_1 angle near +60° will tend to interfere with the solvation of the amide anion. Unhindered rotation to another χ_1 rotamer will generally increase the amide acidity of that residue. For the solvent-exposed amides in FKBP12, ubiquitin, and CI2, whenever the C$^\gamma$ atom of that residue is gauche to both the backbone nitrogen and carbonyl carbon and an unhindered rotation to the trans rotamer is feasible, the acidity of that residue is calculated in the trans conformation.

In marked contrast to the other residue types, the smaller O$^\gamma$ of serine and threonine is often observed in the gauche$^+$ χ_1 rotamer. Of more fundamental relevance to the present continuum dielectric calculations is the placement of the hydroxyl hydrogen. The assumption of limited protein conformational reorganization during the lifetime of the peptide anion surely can not apply generally to the side chain hydroxyl hydrogens since the analogous reorientation of the hydrogens of water gives rise to the dominant dielectric shielding of that phase. Particularly for side chain hydroxyl hydrogens that are not involved in an intramolecular hydrogen bond, continuum dielectric calculations based on a fixed orientation are potentially misleading. This is most notably the case when amide acidity is estimated with an intraresidue serine or threonine hydroxyl in either a gauche$^+$ or gauche$^-$ χ_1 rotamer. In these two rotamers, the hydroxyl hydrogen can potentially form a hydrogen bond to the backbone nitrogen, predicting a large stabilization of the peptide anion. On the other hand, the hydroxyl hydrogen might also be oriented away from the nitrogen with a resultant predicted pK value that is higher by 3 or more units. Given that the exchange rates are similar for serine- and threonine-containing model peptides, as compared to the alanine reference (*65*), the side chain hydroxyl does not generally serve as a catalyst for peptide hydrogen exchange. Consistent with that observation, the following peptide acidity analysis for serine and threonine residues with a gauche χ_1 rotamer assumes that the dielectric shielding of the side chain hydroxyl is equal to that of the equivalent volume of water. In such cases, the serine side chain is computationally truncated to alanine, and threonine is tranformed into α-aminobutyrate.

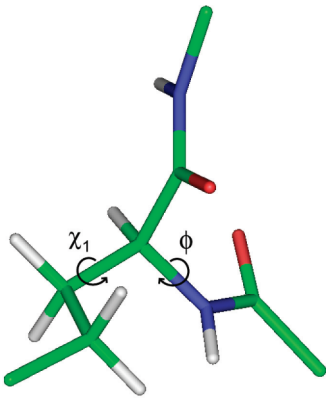

FIGURE 3: Side chain−amide steric interaction in the gauche$^+$ χ_1 side chain conformation. In standard bond geometry, with the ϕ main chain torsion angle set to −90° and the χ_1 side chain torsion angle set to +60°, the C$^\gamma$ atom is positioned only 2.59 Å from the amide hydrogen.

Electrostatic Parameter Set Dependence in Protein Hydrogen Exchange Prediction. Poisson−Boltzmann calculations were carried out on the 1.50 Å resolution structure of CI2 (PDB code 1LW6 (*41*), E26A variant) with the CHARMM22 atomic charge and radius parameters (*8*), assuming internal and solvent dielectric values of 3 and 78.5, respectively. The excess negative charge of the peptide anion was assumed to be localized on the amide nitrogen, as has been found to be effective in previous continuum dielectric analyses of peptides (*6*, *49*, *66*) and proteins (*2*). The predicted pK values for the amide hydrogens having static solvent-accessible surface areas (*50*) >0.5 Å^2 were correlated against the experimental hydroxide-catalyzed exchange rate constants for these residues, yielding a 0.71 rmsd for the log rate constants (Figure 4A).

Although these dielectric continuum calculations directly yield only differential pK values, the experimentally demonstrated (*15*, *16*) normal Eigen acidity (*17*) exhibited by amides provides the basis for placing these peptide acidities on an absolute pK scale. For a normal Eigen acid that is appreciably less acidic than water, the fraction of forward-reacting encounters $K_i/(K_i+1)$ simplifies to K_i, the equilibrium constant for the transfer of a proton from the amide to an hydroxide ion. At 25 °C, the pK of water is 15.7, and the diffusion-limited hydrogen exchange rate for secondary amides is 2×10^{10} M^{-1} s^{-1} (log rate constant 10.3) (*15*, *16*). As a result, an amide having an hydroxide-catalyzed rate constant of 1.0 will have a pK value of 26.0. As illustrated in Figure 4, a least-squares fit of unit slope to the experimental

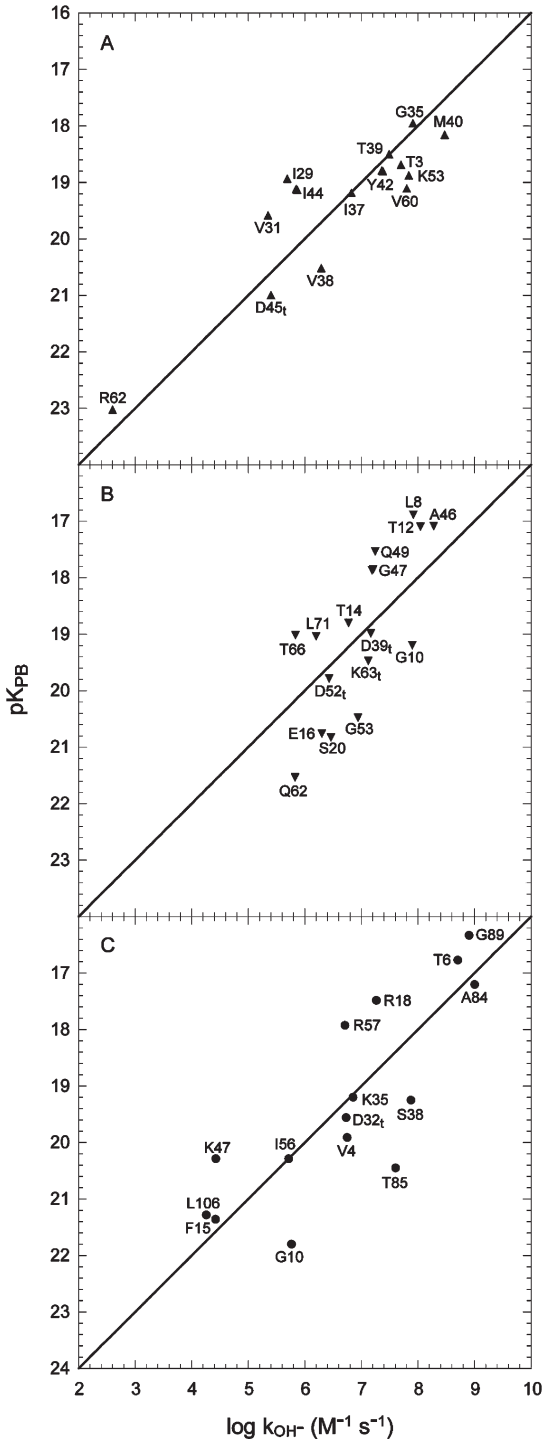

FIGURE 4: Correlation of hydroxide-catalyzed hydrogen exchange rate constants with Poisson−Boltzmann-derived p*K* values (electrostatic solvation free energy in units of kT/ln[10]) using CHARMM22 electrostatic parameters with an internal dielectric constant of 3 at 25 °C for CI2 (A), ubiquitin (B), and FKBP12 (C). C^{γ}-bearing residues having a χ_1 side chain torsion angle near +60° or an aspartate χ_1 torsion angle near −60° and that were rotated to the unhindered trans rotamer for the amide acidity calculation on that residue are indicated by subscript.

protein exchange rate constants provides a referencing of the predicted amide p*K* scale.

Analogous continuum dielectric calculations were carried out on the 1.00 Å resolution structure of ubiquitin (K29Q variant; coordinates kindly provided by S. Ramaswamy and A. D. Robertson, previously cited (*43*)). These correlated with

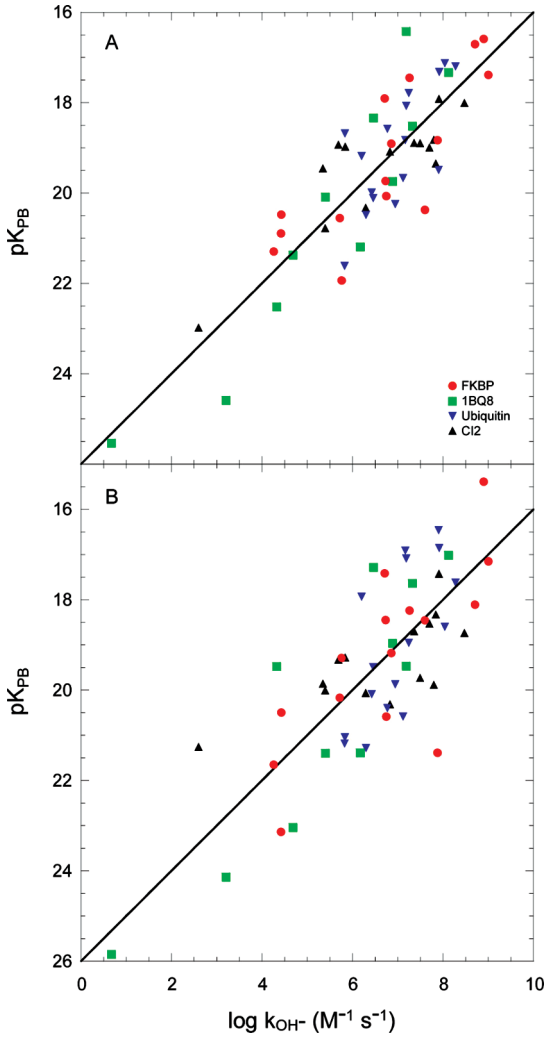

FIGURE 5: Correlation of hydroxide-catalyzed hydrogen exchange rate constants with Poisson−Boltzmann-derived p*K* values, using OPLS-AA (A) and PARSE (B) electrostatic parameters and an internal dielectric constant of 3 at 25 °C.

experimental log k_{OH^-} values to within an rmsd value of 0.96 (Figure 4C). A 0.92 Å resolution X-ray structure of FKBP12 (PDB code 2PPN (*30*)) was used to predict the amide acidities which likewise correlated with the observed exchange rate constants to an rmsd value of 0.98 (Figure 4C).

To test the dependence of these predictions on the electrostatic parameter set, analogous calculations were carried out on rubredoxin (*2*), FKBP12, ubiquitin, and CI2 using the OPLS-AA atomic charge and radius values (*45*). In addition to the aspartate χ_1 side chain reorientation criterion, the exchange data for Ser 25 and Ser 47 of rubredoxin were reanalyzed according to the side chain hydroxyl−water shielding equivalence assumption. As previously discussed (*2*), the data for *Pf* rubredoxin Ile 12, adjacent to the metal binding site, were not included. With that exception, these 56 residues represent the complete set of static solvent exposed amides in these four proteins, excluding only the conformationally disordered C-termini of ubiquitin and rubredoxin and the residue adjacent to the positively charged N-terminus of each protein. As indicated in Figure 5A, the 0.94 rmsd for the deviations from the experimental log k_{OH^-} values predicted by the OPLS-AA electrostatic parameters for the solvent-exposed amides is quite similar to the fit obtained with the CHARMM22 parameters (0.93 rmsd).

Despite the much larger range of deviations from the model reference pK values, accuracy of these amide acidity predictions compares quite favorably with the accuracy of analogous continuum dielectric predictions for side chain ionizations (*9*, *67*). The superior performance of the present amide acidity predictions is particularly striking, since as discussed below, the ΔpK values are inversely proportional to the internal dielectric value used. As compared to most side chain titration analyses, the far lower internal dielectric value used in these amide anion calculations implies a much greater sensitivity to the geometry of the protein structure.

The similarity between the predictions obtained for the CHARMM22 and OPLS-AA parameter sets reflects the similarity in the atomic charge parameters for these two force fields. For the atoms of the peptide group, CHARMM22 and OPLS-AA assume charges of −0.51 and −0.50 for O, 0.51 and 0.50 for C, −0.47 and −0.50 for N, and 0.31 and 0.30 for H, respectively. Many of the other protein atom types are also assigned similar partial charges in these two parameter sets. Furthermore, the critical radius parameter for the ionizing nitrogen atom is essentially identical for the CHARM22 and OPLS-AA force fields, as well as for the AMBER parm99 (*47*) and ff03 (*48*) force fields considered below.

The PARSE electrostatic parameter set (*46*), which was explicitly developed for Poisson−Boltzmann analyses, assumes peptide atomic charges of −0.55, 0.55, −0.4, and 0.4 for O, C, N, and H, respectively, yielding a 4-fold larger mean absolute deviation from the CHARMM22 parameter values than is seen for the OPLS-AA parameter set. Furthermore, in contrast to the other force fields considered, in the PARSE parameter set most aliphatic side chain carbon and hydrogen positions are assumed to be neutral. As illustrated in Figure 5B, the PARSE parameter set yields appreciably weaker correlation with the experimental hydrogen exchange rate constants than is obtained by either the CHARMM22 or OPLS-AA parameter sets, with an rmsd for the deviations from the experimental log k_{OH^-} values of 1.23.

As seen in Figure 6, the parm99 electrostatic parameters from the AMBER force field do not reliably predict the experimental hydrogen exchange data. Many of the outlying predicted values arise from peptide groups that have neighboring charged side chains. In contrast to each of the other parameter sets considered above, the parm99 set does not assume that the charges on the O, C, N, and H of the peptide group are common to every residue type. The corresponding atomic radii of the parm99 set do not vary by residue type. For the aspartate and glutamate residues, the parm99 set assumes that, relative to the atomic charges of the neutral amino acid types, the backbone carbonyl group bears 7.5% of the side chain formal negative charge, while together the backbone nitrogen and amide hydrogen bear an additional 7.9%. Similarly, for the positively charged side chains, 11.5% of the formal charge of the side chain is assumed to reside on the backbone carbonyl group and an additional 7.1% of the formal charge resides on the backbone nitrogen and amide hydrogen.

Although the partial charges of the AMBER force field are derived by fitting to the distribution of the ab initio-derived electrostatic potential surrounding each atom (*68*), the projection of these charges onto each nucleus operationally corresponds to a modeling of chemical induction effects. Earlier studies have proposed that chemical induction (*15*, *65*, *69*) and kinetic steric effects for the branched side chains (*65*) are responsible for the variations in hydrogen exchange rates that arise from substitution of amino acid side chains into simple model peptides.

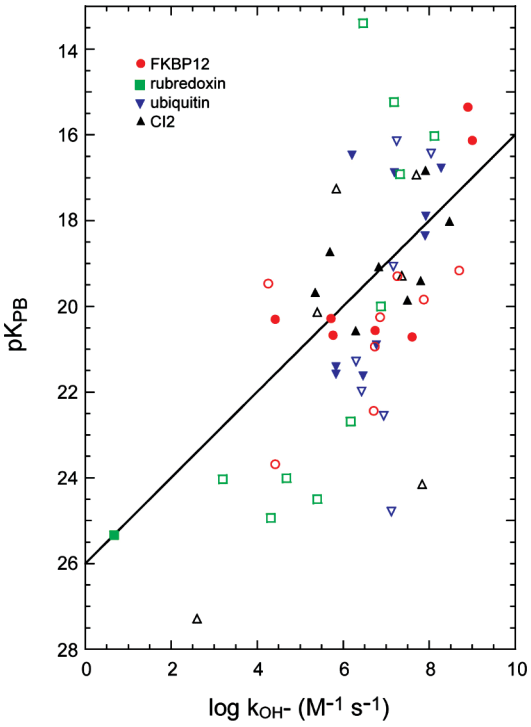

FIGURE 6: Correlation of hydroxide-catalyzed hydrogen exchange rate constants with Poisson−Boltzmann-derived pK values using AMBER parm99 electrostatic parameters and an internal dielectric constant of 3 at 25 °C. The open symbols represent amides for which either of the two neighboring side chains is ionized. Amides with neutral neighboring side chains were used to calibrate the predicted pK values.

In contrast, more recent continuum dielectric studies have argued that the variations among model peptide exchange rates primarily arise from differences in the electrostatic solvation free energy (*6*, *7*), as is assumed in the present analysis. The concurrence between the predicted and observed protein amide acidities in our study is not sufficiently precise to warrant the exclusion of all contributions from chemical induction to the variations in hydrogen exchange rates. However, the magnitude of charge migration within the individual amino acids that is modeled into the AMBER parm99 electrostatic parameter set appears to be well beyond what might be needed to rationalize local sequence-dependent variations.

More recently, the nonpolarizable AMBER electrostatic parameter set has been recalibrated using higher level ab initio calculations (*48*). In that study, the differences in partial charges assigned to nominally similar atoms were markedly increased. As an illustration, the backbone nitrogen of Thr was assigned a charge of −0.245, while that of Ser bears a charge of −0.541. The backbone H, C, and O atoms of Val were assigned charges of 0.440, 0.447, and −0.405, while the corresponding partial charges of Ile were 0.329, 0.569, and −0.620, respectively. When applied to the Poisson−Boltzmann analysis of the present set of four proteins, the electrostatic parameters of the AMBER ff03 force field predict a 10^{21}-fold range in peptide acidities for the 10^9-fold range in hydrogen exchange rates, overall failing to provide a useful correlation to these experimental data.

Charge Distribution in the Peptide Anion. The Poisson−Boltzmann calculations described above assume that the excess negative charge density arising from peptide ionization is localized on the amide nitrogen. Such a charge distribution might seem surprising when one considers the classical valence bond

resonance model of the peptide bond, in which negative charge density is transferred from the nitrogen to the carbonyl oxygen so as to form an imidate-type resonance structure. In fact, even with respect to the neutral amide, a long-running debate continues as to how much of the C−N bond rotational barrier arises from such resonance stabilization (*70*, *71*). Although comparatively few studies have addressed the electronic structure of the peptide anion, the imidate model has been commonly assumed. High-level quantum mechanical calculations predicting the absence of an increased barrier to C−N bond rotation for the peptide anion (*72*), as would be expected from the increased double bond character of the imidate form, have been dismissed as unreliable (*73*).

Our experimental hydrogen exchange data provide an effective test for assessing the spatial distribution of the excess negative charge for the peptide anion. When the Poisson−Boltzmann calculations of peptide acidity for the four proteins of this study are applied with the CHARMM22 parameter set, an internal dielectric value of 3, and placement of the excess negative charge on the carbonyl oxygen of the peptide group, the rmsd with respect to the experimental log k_{OH^-} values increases to 1.94 (Figure 7A). This marked failure to predict the hydrogen exchange data argues strongly against the validity of the simple imidate model for the peptide anion charge distribution.

Nevertheless, localization of the excess negative charge exclusively on the amide nitrogen is clearly physically unrealistic. We have carried out MP2 ab initio and B3LYP (*51*) density functional theory (DFT) calculations on *N*-methylacetamide and its peptide anion, both in vacuum and using a polarizable continuum model (PCM) representation of the surrounding dielectric set to 3 or set to 78.39. Geometry optimization and electron distribution calculations were carried out at the aug-cc-pVDZ and aug-cc-pVTZ basis set levels using the Gaussian03 program (*52*). Although, as often noted, the assignment of net charge to the individual atoms varied significantly among the individual calculations, the differences in atomic charge between neutral *N*-methylacetamide and the *N*-methylacetamide anion were reasonably consistent as a function of the basis set level and the use of either MP2 or DFT calculations. Partitioning of the excess negative charge density by either Mulliken or ESP population analysis led to prediction of a 3-fold larger concentration on the nitrogen atom than on the carbonyl oxygen of the amide anion. B3LYP DFT calculations at the aug-cc-pVTZ basis set level were used to define a CHARMM22-compatible amide anion state with atomic charges of 0.45, −0.63, and −0.84 for the C, O, and N atoms and a decrease of 0.07 for both adjacent C^{α} atoms, consistent with a distribution of 9%, 17%, 54%, and 10% (for each C^{α}), respectively, of the excess negative charge.

As illustrated in Figure 7B, peptide acidity predictions using the DFT-derived peptide charge distribution yield an rmsd of 6.9 for the k_{OH^-} values (0.84 for log k_{OH^-}). This level of agreement represents a modest improvement over the predictions obtained by localization of the charge at the nitrogen atom for all four proteins (rmsd of 8.5 for k_{OH^-}, 0.93 for log k_{OH^-}). When compared to the predictions that result from assuming an imidate charge distribution (Figure 7A), this analysis indicates that the optimal charge distribution of the peptide anion is close to that obtained from placement of the excess negative charge either exclusively on the nitrogen

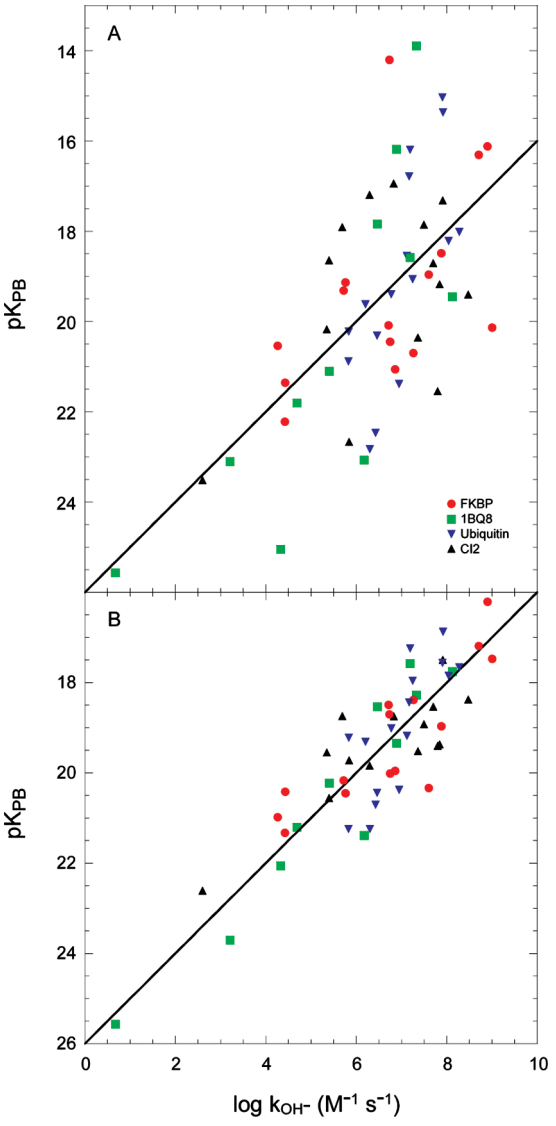

FIGURE 7: Dependence of amide acidity predictions on the atomic charge distribution of the peptide anion. Protein amide p*K* values predicted using CHARMM22 electrostatic parameters and an internal dielectric constant of 3 at 25 °C with the excess anion charge density localized to the carbonyl oxygen (A) or distributed throughout the peptide unit as predicted from B3LYP DFT calculations (B).

or with the DFT-derived charge distribution. Although additional improvement in these continuum dielectric predictions may be obtainable by further refinement of the fixed atomic charges, it would seem likely that the residual errors in prediction of the experimental hydrogen exchange data are dominated by other factors, such as the simplifying assumptions of the Poisson−Boltzmann analysis or inaccuracies in the protein structural modeling paradigm.

Prediction of Amide Acidity in the Absence of a Dielectric Background. In Figure 8 are illustrated the CHARMM22 peptide acidity predictions of the experimental hydrogen exchange data of rubredoxin, FKBP12, ubiquitin, and CI2, assuming an internal dielectric value of 1. The correlation between the predicted range of peptide acidities and the observed hydrogen exchange rate constants clearly indicates that the predicted variation in electrostatic potential at the ionizing nitrogen is approximately 3-fold larger than what is required to accurately predict the exchange data. The inverse dependence of the electrostatic solvation free energy on the value of the internal

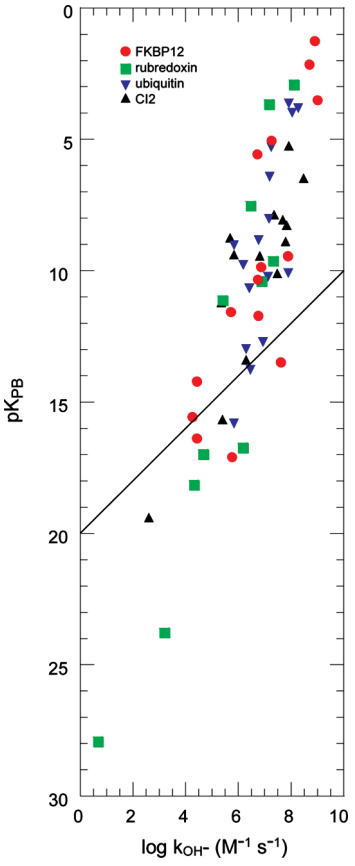

FIGURE 8: Correlation of hydroxide-catalyzed hydrogen exchange rate constants with Poisson−Boltzmann-derived pK values using CHARMM22 electrostatic parameters for the peptide anion and an internal dielectric constant of 1 at 25 °C.

dielectric is anticipated from the generalized Born formula for an ion of charge Q and radius R (*74*):

$$\Delta G_{elec} = -(1/\varepsilon_{int} - 1/\varepsilon_{ext})Q^2/2R$$

In turn, this formula predicts that the electrostatic solvation free energy is weakly dependent on a high dielectric value for the solvent. Such a lack of sensitivity to the effective solvent dielectric value is particularly germane to the present calculations, since the assumption that the peptide anion lifetime approximately equals the time constant for the major dielectric relaxation process of water implies that the effective shielding value for the solvent must be less than the static limit of 78.5. To examine this expectation, the Poisson−Boltzmann calculations of Figure 7B were repeated for all four proteins using a solvent dielectric value of 50, a factor of 1/e from the static limit value. The changes in the individual ΔpK values for these static solvent-exposed amides predicted for $\varepsilon = 50$ vs $\varepsilon = 78.5$ had an rmsd of 0.10, well within the overall anticipated reliability of these continuum dielectric calculations.

In the large majority of applications using nonpolarizable force fields, the electrostatic calculations are carried out assuming no dielectric background. The results summarized in Figure 8 indicate that substantial errors will arise in the spatial distribution of the electrostatic potential predicted in the absence of dielectric shielding. The relatively uniform quality of the hydrogen exchange predictions for these four proteins that are offered by either the CHARMM22 or OPLS-AA electrostatic parameter set supports the expectation that structure-dependent conformational relaxation mechanisms are unlikely to substantially contribute to the effective dielectric shielding of the amide anions. The Poisson−Boltzmann calculations discussed above indicate that an internal dielectric of 3 is needed to predict the solvent-exposed amide pK values. However, these atomic charge and radius parameter sets are optimized to predict electrostatic energies in the absence of a dielectric background.

In the full explicit atom representation of a nonpolarizable force field, the electrostatic energy of the system is standardly calculated as a sum over a set of Coulombic charge pairs, assuming the vacuum dielectric value. The macroscopic expression for this total electrostatic energy is obtained by integration of the energy density $(1/2)\varepsilon(\tau)E(\tau)^2$ over all space. This form of the expression emphasizes the capacitor function of the dielectric as a measure of the energy storage required to establish a given electric field distribution. When a nonpolarizable force field is optimized by hyperpolarizing the charge distribution so as to reproduce the electrostatic energy of a system by a Coulombic summation in vacuo, then necessarily the resultant predicted electric field intensity throughout space will be systematically higher than for the physical system.

The complications that arise from force field optimization that is based on the electrostatic energy at the expense of accuracy in the electric field distribution become most apparent for interactions across interfaces between spatial regions for which differing electrostatic parameter optimizations have been applied. This effect provides insight into why the development of nonpolarizable protein force fields typically require optimization with respect to one specific water model (e.g., TIP3P, SPC/E, or F3C) (*75*), despite the fact that the various water models may provide comparably robust descriptions of the pure solvent phase.

The complications arising from a systematic overestimation of the electrostatic field intensity are particularly problematic for QM/MM calculations. As applied to chemical enzymology, atoms of the substrate and active site region are represented quantum mechanically in the QM subsystem, while the surrounding protein and solvent atoms are modeled classically, as a means of representing the environmental influences impinging upon the QM subsystem. If the distribution of electrostatic potential within the QM subsystem that arises from the classically modeled surroundings is systematically in error, the resultant Hamiltonian for the QM subsystem cannot accurately predict the atomic polarization and electron density transitions that occur during the modeling of catalysis in the QM subsystem.

Although recently developed polarizable force fields have been used for representation of the classical subsystem, nonpolarizable force fields continue to be widely applied for QM/MM calculations of enzymatic catalysis. The CHARMM22, OPLS-AA, AMBER parm99, and AMBER ff03 force fields are all currently being used to model the electrostatic interactions arising from the classically treated protein subsystem, under the assumption of an internal dielectric value $\varepsilon = 1$.

In the context of the present peptide acidity analysis, the recent QM/MM study of Merz and colleagues offers a particularly germane illustration (*76*). In their analysis, solvation free energies were predicted for residues within a series of pentapeptides and within a set of small model proteins. In contrast to the common use of explicit solvent representation in QM/MM calculations, the solvation phase contribution to the electrostatic potential within the QM subsystem was estimated by standard Poisson−Boltzmann methods. The electrostatic contribution from the classical peptide/protein subsystem was represented with the

AMBER parm99 parameter set. The analysis of Merz and colleagues (*76*) primarily focused on the effects of varying the size of the QM subsystem, and they concluded that useful predictions could be obtained even for a single QM residue in the pentapeptide simulations.

The handling of the intersubsystem electrostatics in this pentapeptide study (*76*) closely corresponds to the electrostatic analysis of peptide acidity that we have described above. In particular, consider a "QM" subsystem defined by the atoms within the plane of the ionizing peptide unit. With the exception of minor differences in the C^{α} partial charge for Gly and Pro, this "QM" subsystem is essentially identical for every static solvent-accessible amide in each of the four proteins considered in the present study, when either the CHARMM22 or OPLS-AA electrostatic parameter set is utilized. As a result, the contributions from this "QM" subsystem cancels out in the differential electrostatic solvation free energy calculations that we are reporting, and only the intersubsystem electrostatic interaction arising from the classical protein subsystem and the solvent phase contribute the differences in electrostatic potential predicted at each amide.

The differences between the predicted protein amide acidities, under the assumptions of $\varepsilon_{int} = 3$ (Figure 7B) and $\varepsilon_{int} = 1$ (Figure 8), demonstrate the discrepancies in electrostatic potential within the peptide "QM" subsystem that arise from the neglect of electronic polarizability in the classical region. The magnitude of these discrepancies can be reduced by expanding the size of the QM subsystem. However, since the QM component of these calculations is generally the most calculationally intensive, a substantial expansion of the QM system will often entail the use of a lower level quantum mechanical representation. Furthermore, our analysis of the structural basis of the differences in peptide acidity for *Pf* rubredoxin indicated that a wide range of interactions, extending over a significant distance range, gives rise to the billion-fold variation in hydrogen exchange rates observed among the static solvent-exposed amides (*2*). In particular, within the validity of the present Poisson−Boltzmann analysis, the spatial distribution of the internal dielectric volume provides a significant contribution to the differential acidities of these sites, more than a 4 unit pH variation in the case of *Pf* rubredoxin.

The use of an intramolecular dielectric value has long been criticized as being an overly simplistic means of describing interactions on the atomic scale. Yet in the present context, the physical realism of a uniform internal dielectric representation is surely preferable to the complete neglect of the electric field strength attenuation that arises from electronic polarizability. The contrast between predictions of peptide acidities with and without a background dielectric strongly indicates that electrostatic interactions across the QM/MM boundary would be more accurately represented by assigning an internal dielectric value of 3 to a protein MM subsystem represented by a nonpolarizable force field.

In analyzing the related problem of deconvoluting the contributions from the preorganized protein electrostatic environment from that of the subsequent conformational reorganization as envisioned in the Marcus theory of electron transfer (*24*), Krishtalik and colleagues (*77*) proposed assigning two dielectric values to scale the individual pairwise interactions. Electrostatic interactions between preorganized atomic charges are scaled by the optical dielectric constant to account for electronic polarizability, while the interactions involving the newly formed charge site are scaled by the familiar static dielectric constant so as to incorporate the effects of conformational reorganization. This approach still leaves the practical problem that the standard nonpolarizable atomic charge sets have been optimized for in vacuo Coulombic summations. The atomic charges of a nonpolarized force field can be uniformly scaled to reproduce the experimental dipole moments of model compounds so as to yield a more consistent prediction of electrostatic energy when the internal dielectric values are applied (*78*). A more robust approach may involve directly integrating an atom-based continuum dielectric polarizability into a practical force field representation (*79*).

A polarizable classical force field offers a means to solve the problem of simultaneously obtaining accurate electrostatic energies and electric field distributions. In this context, the Poisson−Boltzmann predictions of Figure 7B provide a powerful test. For each protein, there are 11−16 different amide sites for which an electrostatic modeling algorithm should be able to simultaneously predict the peptide acidities. The experimental uncertainty in the hydroxide-catalyzed rate constants reported in this study is more than an order of magnitude smaller than the precision of our Poisson−Boltzmann predictions, indicating that these data offer substantial utility in testing more accurate modeling approaches. If a given polarizable force field is unable to predict these protein amide acidities to at least the precision provided by a continuum dielectric analysis using nonpolarizable atomic charges, it is left unclear whether such a polarizable model can offer an improved accuracy in representing the electrostatic potential distribution within a QM subsystem that arises from the interactions with the classical region.

CONCLUSION

To date, we have identified four proteins for which the acidities of the static solvent-exposed amides are robustly predictable within the Poisson−Boltzmann continuum dielectric paradigm applied to nonpolarizable electrostatic force field parameters. The resultant effective dielectric shielding value is consistent with a dominant contribution from electronic polarizability. In addition to providing a basis for discrimination among alternative nonpolarizable electrostatic parameter sets, these data can offer a testbed for assessing the reliability of specific polarizable force field representations.

It must be emphasized that not all protein systems can be expected to yield comparably accurate predictions of peptide acidities for the amide hydrogens that are exposed to solvent in high-resolution X-ray structures. Using the Val 38 amide of *Pf* rubredoxin as an illustration, we (*2*) have pointed out that the 10^7-fold attenuation in exchange rate that is observed for this static solvent-accessible amide implies that the conformational sampling which occurs within the native state manifold must be sufficiently limited in the region surrounding this residue so that any transient conformation of the Val 38 amide that has a substantially higher intrinsic acidity must be very weakly populated. Clearly, a protein which exhibits a high degree of conformational plasticity at its surface can have hydrogen exchange rates that are dominated by transient conformations, even for amides that are solvent-exposed in the ground state conformation.

The continuum dielectric analysis of the hydrogen exchange data reported in this study illustrates the systematic overestimation of electrostatic field intensity that can arise from the

standard use of fixed atomic charges in classical force fields which in turn will yield overpolarization of the quantum mechanically treated region in QM/MM simulations. This analysis offers an approach to the more optimal use of currently available force field representations for such QM/MM applications, and this experimental peptide acidity data set should provide valuable in evaluating future developments in the modeling of electrostatic interactions.

ACKNOWLEDGMENT

We acknowledge the use of the Wadsworth Center NMR facility and the DNA Sequencing Core as well as the technical assistance of Lynn McNaughton.

SUPPORTING INFORMATION AVAILABLE

Three tables showing the hydroxide-catalyzed hydrogen exchange rate constants at 25 °C and 0.15 M ionic strength for the static solvent-accessible amides of FKBP12 (Table S1), ubiquitin (Table S2), and CI2 (Table S3). This material is available free of charge via the Internet at http://pubs.acs.org.

REFERENCES

1. Bai, Y. W., Milne, J. S., Mayne, L., and Englander, S. W. (1994) Protein stability parameters measured by hydrogen exchange. *Proteins: Struct., Funct., Genet. 20*, 4–14.
2. Anderson, J. S., Hernández, G., and LeMaster, D. M. (2008) A billion-fold range in acidity for the solvent-exposed amides of *Pyrococcus furiosus* rubredoxin. *Biochemistry 47*, 6178–6188.
3. Hernández, G., Anderson, J. S., and LeMaster, D. M. (2008) Electrostatic stabilization and general base catalysis in the active site of the human protein disulfide isomerase a domain monitored by hydrogen exchange. *ChemBioChem 9*, 768–778.
4. Huyghes-Despointes, B. M. P., Scholtz, J. M., and Pace, C. N. (1999) Protein conformational stabilities can be determined from hydrogen exchange rates. *Nat. Struct. Biol. 6*, 910–912.
5. Hollien, J., and Marqusee, S. (2002) Comparison of the folding processes of *T. thermophilus* and *E. coli* ribonucleases H. *J. Mol. Biol. 316*, 327–340.
6. Fogolari, F., Esposito, G., Viglino, P., Briggs, J. M., and McCammon, J. A. (1998) pK_a shift effects on backbone amide base-catalyzed hydrogen exchange rates in peptides. *J. Am. Chem. Soc. 120*, 3735–3738.
7. Avbelj, F., and Baldwin, R. L. (2004) Origin of the neighboring residue effect on peptide backbone conformation. *Proc. Natl. Acad. Sci. U.S.A. 101*, 10967–10972.
8. MacKerell, A. D., Bashford, D., Bellott, M., Dunbrack, R. L., Evanseck, J. D., Field, M. J., Fischer, S., Gao, J., Guo, H., Ha, S., Joseph-McCarthy, D., Kuchnir, L., Kuczera, K., Lau, F. T. K., Mattos, C., Michnick, S., Ngo, T., Nguyen, D. T., Prodhom, B., Reiher, W. E., Roux, B., Schlenkrich, M., Smith, J. C., Stote, R., Straub, J., Watanabe, M., Wiorkiewicz-Kuczera, J., Yin, D., and Karplus, M. (1998) All-atom empirical potential for molecular modeling and dynamics studies of proteins. *J. Phys. Chem. B 102*, 3586–3616.
9. Antosiewicz, J., McCammon, J. A., and Gilson, M. K. (1996) The determinants of pK_as in proteins. *Biochemistry 35*, 7819–7833.
10. Demchuk, E., and Wade, R. C. (1996) Improving the continuum dielectric approach to calculating pK_a's of ionizable groups in proteins. *J. Phys. Chem. 100*, 17373–17387.
11. Garcia-Moreno, B., Dwyer, J. J., Gittis, A. G., Lattman, E. E., Spencer, D. S., and Stites, W. E. (1997) Experimental measurement of the effective dielectric in the hydrophobic core of a protein. *Biophys. Chem. 64*, 211–224.
12. Simonson, T., and Perahia, D. (1995) Internal and interfacial dielectric properties of cytochrome *c* from molecular dynamics in aqueous solution. *Proc. Natl. Acad. Sci. U.S.A. 92*, 1082–1086.
13. Harms, M. J., Schlessman, J. L., Chimenti, M. S., Sue, G. R., Damjanovic, A., and García-Moreno, B. E. (2008) A buried lysine that titrates with a normal pK_a: Role of conformational flexibility at the protein-water interface as a determinant of pK_a values. *Protein Sci. 17*, 833–845.
14. Prakash, M. K., and Marcus, R. A. (2007) An interpretation of fluctuations in enzyme catalysis rate, spectral diffusion, and radiative component of lifetimes in terms of electric field fluctuations. *Proc. Natl. Acad. Sci. U.S.A. 104*, 15982–15987.
15. Molday, R. S., and Kallen, R. G. (1972) Substituent effects on amide hydrogen exchange rates in aqueous solution. *J. Am. Chem. Soc. 94*, 6739–6745.
16. Wang, W. H., and Cheng, C. C. (1994) General base catalyzed proton exchange in amides. *Bull. Chem. Soc. Jpn. 67*, 1054–1057.
17. Eigen, M. (1964) Proton transfer, acid-base catalysis, and enzymatic hydrolysis. (I) Elementary processes. *Angew. Chem., Int. Ed. 3*, 1–19.
18. Tolbert, L. M., and Solntsev, K. M. (2002) Excited-state proton transfer: from constrained systems to "super" photoacids to superfast proton transfer. *Acc. Chem. Res. 35*, 19–27.
19. Leiderman, P., Genosar, L., and Huppert, D. (2005) Excited-state proton transfer: Indication of three steps in the dissociation and recombination process. *J. Phys. Chem. A 109*, 5965–5977.
20. Park, H. J., Kwon, O. H., Ah, C. S., and Jang, D. J. (2005) Excited-state tautomerization dynamics of 7-hydroxyquinoline in β-cyclodextrin. *J. Phys. Chem. B 109*, 3938–3943.
21. Luz, Z., and Meiboom, S. (1964) The activation energies of proton transfer reactions in water. *J. Am. Chem. Soc. 86*, 4768–4769.
22. LeMaster, D. M., Anderson, J. S., and Hernández, G. (2007) Spatial distribution of dielectric shielding in the interior of *Pyrococcus furiosus* rubredoxin as sampled in the subnanosecond timeframe by hydrogen exchange. *Biophys. Chem. 129*, 43–48.
23. Ellison, W. J., Lamkaouchi, K., and Moreau, J. M. (1996) Water: A dielectric reference. *J. Mol. Liq. 68*, 171–279.
24. Marcus, R. A. (1964) Electrochemical electron-transfer theory. *Annu. Rev. Phys. Chem. 15*, 155–196.
25. Richards, F. M. (1974) The interpretation of protein structures: Total volume, group volume distributions and packing density. *J. Mol. Biol. 82*, 1–14.
26. Tsai, J., Taylor, R., Chothia, C., and Gerstein, M. (1999) The packing density in proteins: Standard radii and volumes. *J. Mol. Biol. 290*, 253–266.
27. Mertz, E. L., and Krishtalik, L. I. (2000) Low dielectric response in enzyme active site. *Proc. Natl. Acad. Sci. U.S.A. 97*, 2081–2086.
28. Hawranek, J. P., Wrzeszcz, W., Muszyński, A. S., and Pajdowska, M. (2002) Infrared dispersion of liquid triethylamine. *J. Non-Cryst. Solids 305*, 62–70.
29. Altschul, S. F., Madden, T. L., Schaffer, A. A., Zhang, J., Zhang, Z., Miller, W., and Lipman, D. J. (1997) Gapped BLAST and PSI-BLAST: a new generation of protein database search programs. *Nucleic Acids Res. 25*, 3389–3402.
30. Szep, S., Park, S., Boder, E. T., VanDuyne, G. D., and Saven, J. G. (2008) Structural coupling between FKBP12 and buried water. *Proteins 74*, 603–611.
31. McPhalen, C. A., and James, M. N. G. (1987) Crystal and molecular structure of the serine proteinase inhibitor CI-2 from barley seeds. *Biochemistry 26*, 261–269.
32. Jackson, S. E., Moracci, M., elMasry, N., Johnson, C. M., and Fersht, A. R. (1993) Effect of cavity-creating mutations in the hydrophobic core of chymotrypsin inhibitor 2. *Biochemistry 32*, 11259–11269.
33. Hernández, G., and LeMaster, D. M. (2001) Reduced temperature dependence of collective conformational opening in a hyperthermophile rubredoxin. *Biochemistry 40*, 14384–14391.
34. Russo, A. T., Rosgen, J., and Bolen, D. W. (2003) Osmolyte effects on kinetics of FKBP12 C22A folding coupled with prolyl isomerization. *J. Mol. Biol. 330*, 851–866.
35. Lazar, G. A., Desjarlais, J. R., and Handel, T. M. (1997) De novo design of the hydrophobic core of ubiquitin. *Protein Sci. 6*, 1167–1178.
36. Hwang, T. L., vanZijl, P. C. M., and Mori, S. (1998) Accurate quantitation of water-amide proton exchange rates using the phase-modulated CLEAN chemical EXchange (CLEANEX-PM) approach with a Fast-HSQC (FHSQC) detection scheme. *J. Biomol. NMR 11*, 221–226.
37. Hernández, G., and LeMaster, D. M. (2003) Relaxation compensation in chemical exchange measurements for the quantitation of amide hydrogen exchange in larger proteins. *Magn. Reson. Chem. 41*, 699–702.
38. LeMaster, D. M., Tang, J., Paredes, D. I., and Hernández, G. (2005) Enhanced thermal stability achieved without increased conformational rigidity at physiological temperatures: Spatial propagation of differential flexibility in rubredoxin hybrids. *Proteins 61*, 608–616.
39. Word, J. M., Lovell, S. C., Richardson, J. S., and Richardson, D. C. (1999) Asparagine and glutamine: Using hydrogen atom contacts in the choice of side-chain amide orientation. *J. Mol. Biol. 285*, 1733–1747.
40. Bau, R., Rees, D. C., Kurtz, D. M., Scott, R. A., Huang, H. S., Adams, M. W. W., and Eidsness, M. K. (1998) Crystal-structure of

rubredoxin from *Pyrococcus furiosus* at 0.95 angstrom resolution, and the structures of N-terminal methionine and formylmethionine variants of *Pf* Rd. Contributions of N-terminal interactions to thermostability. *J. Biol. Inorg. Chem. 3*, 484–493.
41. Radisky, E. S., and Koshland, D. E.Jr. (2002) A clogged gutter mechanism for protease inhibitors. *Proc. Natl. Acad. Sci. U.S.A. 99*, 10316–10321.
42. Jorgensen, W. L., Chandrasekhar, J., Madura, J. D., Impey, R. W., and Klein, M. L. (1983) Comparison of simple potential functions for simulating liquid water. *J. Chem. Phys. 79*, 926–935.
43. Parker, L. L., Houk, A. R., and Jensen, J. H. (2006) Cooperative hydrogen bonding effects are key determinants of backbone amide proton chemical shifts in proteins. *J. Am. Chem. Soc. 128*, 9863–9872.
44. Rocchia, W., Sridharan, S., Nicholls, A., Alexov, E., Chiabrera, A., and Honig, B. (2002) Rapid grid-based construction of the molecular surface and the use of induced surface charge to calculate reaction field energies: Applications to the molecular systems and geometric objects. *J. Comput. Chem. 23*, 128–137.
45. Jorgensen, W. L., Maxwell, D. S., and Tirado-Rives, J. (1996) Development and testing of the OPLS all-atom force field on conformational energetics and properties of organic liquids. *J. Am. Chem. Soc. 118*, 11225–11236.
46. Sitkoff, D., Sharp, K. A., and Honig, B. (1994) Accurate calculation of hydration free energies using macroscopic solvent models. *J. Phys. Chem. 98*, 1978–1988.
47. Cheatham, T. E., Cieplak, P., and Kollman, P. A. (1999) A modified version of the Cornell et al. force field with improved sugar pucker phases and helical repeat. *J. Biomol. Struct. Dyn. 16*, 845–862.
48. Duan, Y., Wu, C., Chowdhury, S., Lee, M. C., Xiong, G. M., Zhang, W., Yang, R., Cieplak, P., Lou, R., Lee, T., Caldwell, J., Wang, J. M., and Kollman, P. (2003) A point-charge force field for molecular mechanics simulations of proteins based on condensed-phase quantum mechanical calculations. *J. Comput. Chem. 24*, 1999–2012.
49. Anderson, J. S., Hernández, G., and LeMaster, D. M. (2009) Backbone conformational dependence of peptide acidity. *Biophys. Chem. 141*, 124–130.
50. Lee, B., and Richards, F. M. (1971) The interpretation of protein structures: estimation of static accessibility. *J. Mol. Biol. 55*, 379–400.
51. Becke, A. D. (1993) Density-functional thermochemistry III. The role of exact exchange. *J. Chem. Phys. 98*, 5648–5652.
52. Frisch, M. J., Trucks, G. W., Schlegel, H. B., Scuseria, G. E., Robb, M. A., Cheeseman, J. R., Montgomery, J. A., Vreven, T., Kudin, K. N., Burant, J. C., Millam, J. M., Iyengar, S. S., Tomasi, J., Barone, V., Mennucci, B., Cossi, M., Scalmani, G., Rega, N., Petersson, G. A., Nakatsuji, H., Hada, M., Ehara, M., Toyota, K., Fukuda, R., Hasegawa, J., Ishida, M., Nakajima, T., Honda, Y., Kitao, O., Nakai, H., Klene, M., Li, X., Knox, J. E., Hratchian, H. P., Cross, J. B., Bakken, V., Adamo, C., Jaramillo, J., Gomperts, R., Stratmann, R. E., Yazyev, O., Austin, A. J., Cammi, R., Pomelli, C., Ochterski, J. W., Ayala, P. Y., Morokuma, K., Voth, G. A., Salvador, P., Dannenberg, J. J., Zakrzewski, V. G., Dapprich, S., Daniels, A. D., Strain, M. C., Farkas, O., Malick, D. K., Rabuck, A. D., Raghavachari, K., Foresman, J. B., Ortiz, J. V., Cui, Q., Baboul, A. G., Clifford, S., Cioslowski, J., Stefanov, B. B., Liu, G., Liashenko, A., Piskorz, P., Komaromi, I., Martin, R. L., Fox, D. J., Keith, T., Al-Laham, M. A., Peng, C. Y., Nanayakkara, A., Challacombe, M., Gill, P. M. W., Johnson, B., Chen, W., Wong, M. W., Gonzalez, C., Pople, J. A. (2004) Gaussian 03, Revision C.02, Gaussian Inc., Wallingford, CT.
53. Mennucci, B., and Martinez, J. M. (2005) How to model solvation of peptides? Insights from a quantum-mechanical and molecular dynamics study of N-methylacetamide. 1. *J. Phys. Chem. B 109*, 9818–9829.
54. Tan, Y. J., Oliveberg, M., Davis, B., and Fersht, A. R. (1995) Perturbed pK_a-values in the denatured states of proteins. *J. Mol. Biol. 254*, 980–992.
55. Sundd, M., Iverson, N., Ibarra-Molero, B., Sanchez-Ruiz, J. M., and Robertson, A. D. (2002) Electrostatic interactions in ubiquitin: Stabilization of carboxylates by lysine amino groups. *Biochemistry 41*, 7586–7596.
56. Schneider, D. M., Dellwo, M. J., and Wand, A. J. (1992) Fast internal main-chain dynamics of human ubiquitin. *Biochemistry 31*, 3645–3652.
57. Yu, L., and Fesik, S. W. (1994) pH titration of the histidine residues of cyclophilin and FK506 binding protein in the absence and presence of immunosuppressant ligands. *Biochim. Biophys. Acta 1209*, 24–32.
58. Ibarra-Molero, B., Loladze, V. V., Makhatadze, G. I., and Sanchez-Ruiz, J. M. (1999) Thermal versus guanidine-induced unfolding of ubiquitin. An analysis in terms of the contributions from charge-charge interactions to protein stability. *Biochemistry 38*, 8138–8149.
59. Ugurbil, K., and Mitra, S. (1985) ^{1}H NMR studies of electron exchange rate of *Pseudomonas aeruginosa*. *Proc. Natl. Acad. Sci. U.S.A. 82*, 2039–2043.
60. Watt, E. D., Shimada, H., Kovrigin, E. L., and Loria, J. P. (2007) The mechanism of rate-limiting motions in enzyme function. *Proc. Natl. Acad. Sci. U.S.A. 104*, 11981–11986.
61. Rotzschke, O., Lau, J. M., Hofstatter, M., Falk, K., and Strominger, J. L. (2002) A pH-sensitive histidine residue as control element for ligand release from HLA-DR molecules. *Proc. Natl. Acad. Sci. U.S.A. 99*, 16946–16950.
62. You, T. J., and Bashford, D. (1995) Conformation and hydrogen ion titration of proteins: A continuum electrostatic model with conformational flexibility. *Biophys. J. 69*, 1721–1733.
63. vanVlijmen, H. W. T., Schaefer, M., and Karplus, M. (1998) Improving the accuracy of protein pK_a calculations: Conformational averaging versus the average structure. *Proteins 33*, 145–158.
64. Fitzkee, N. C., Fleming, P. J., and Rose, G. D. (2005) The protein coil library: A structural database of nonhelix, nonstrand fragments derived from the PDB. *Proteins 58*, 852–854.
65. Bai, Y. W., Milne, J. S., Mayne, L., and Englander, S. W. (1993) Primary structure effects on peptide group hydrogen-exchange. *Proteins: Struct., Funct., Genet. 17*, 75–86.
66. Avbelj, F., and Baldwin, R. L. (2009) Origin of the change in solvation enthalpy of the peptide group when neighboring peptide groups are added. *Proc. Natl. Acad. Sci. U.S.A. 106*, 3137–3141.
67. Georgescu, R. E., Alexov, E. G., and Gunner, M. R. (2002) Combining conformational flexibility and continuum electrostatics for calculating pK_as in proteins. *Biophys. J. 83*, 1731–1748.
68. Bayly, C. I., Cieplak, P., Cornell, W. D., and Kollman, P. A. (1993) A well behaved electrostatic potential-based method using charge restraints for deriving atomic charges: The RESP model. *J. Phys. Chem. 97*, 10269–10280.
69. Sheinblatt, M. (1970) Determination of an acidity scale for peptide hydrogens from nuclear magnetic resonance kinetic studies. *J. Am. Chem. Soc. 92*, 2505–2509.
70. Wiberg, K. B., and Laidig, K. E. (1987) Barriers to rotation adjacent to double bonds. 3. The carbon-oxygen barrier in formic acid, methyl formate, acetic acid, and methyl acetate. The origin of ester and amide resonance. *J. Am. Chem. Soc. 109*, 5935–5943.
71. Kemmitz, C. R., and Loewen, M. J. (2007) "Amide resonance" correlates with a breath of C-N rotational barriers. *J. Am. Chem. Soc. 129*, 2521–2528.
72. Nguyen, M. T., and Hegarty, A. F. (1986) Imidate anions: E/Z interconversion by rotation vs. nitrogen inversion?. *J. Org. Chem. 51*, 4703–4706.
73. Perrin, C. L., and Thoburn, J. D. (1989) Mechanism of E/Z stereoisomerization of imidate anions. *J. Org. Chem. 54*, 764–767.
74. Schaefer, M., and Karplus, M. (1996) A comprehensive analytical treatment of continuum electrostatics. *J. Phys. Chem. 100*, 1578–1599.
75. MacKerell, A. D., Feig, M., and Brooks, C. L. (2004) Extending the treatment of backbone energetics in protein force fields: Limitations of gas-phase quantum mechanics in reproducing protein conformational distributions in molecular dynamics. *J. Comput. Chem. 25*, 1400–1415.
76. Hayik, S. A., Liao, N., and Merz, K. M.Jr. (2008) A combined QM/MM Poisson-Boltzmann approach. *J. Chem. Theory Comput. 4*, 1200–1207.
77. Krishtalik, L. I., Kuznetsov, A. M., and Mertz, E. L. (1997) Electrostatics of proteins: Description in terms of two dielectric constants simultaneously. *Proteins 28*, 174–182.
78. Krishtalik, L. I. (2005) Continuum electrostatics of proteins: Experimental test with model solvents and the method of the proteins p*K* calculations. *Chem. Phys. 319*, 316–329.
79. Truchon, J. F., Nicholls, A., Iftimie, R. I., Roux, B., and Bayly, C. I. (2008) Accurate molecular polarizabilities based on continuum electrostatics. *J. Chem. Theory Comput. 4*, 1480–1493.